scientific reports

Check for updates

OPEN

# Constructing a prognostic model for osteosarcoma based on centrosome-related genes and identifying potential therapeutic targets of paclitaxel

Yujian Zhong[1,5], Bohua Gao[2,3,5], Kai Tong[1,5], Lan Li[1], Qingjun Wei[4]✉ & Yong Hu[1]✉

**The centrosome, a vital component in mitosis in eukaryotes, plays a pivotal role in cancer progression by influencing the proliferation and differentiation of malignant cells, making it a significant therapeutic target. We collected genes associated with centrosomes from existing literature and established a prognostic model for 85 osteosarcoma patients from the TARGET database. Genes associated with prognosis were identified through univariate Cox regression. We then mitigated overfitting by addressing collinearity using LASSO regression. Ultimately, a set of five genes was selected for the model through multivariable Cox regression. Model performance was assessed using ROC curves, which yielded a training set AUC of 0.965 and a validation set AUC of 0.770, indicating satisfactory model performance. We further identified genes with differential expression in high and low-risk groups and conducted functional enrichment analysis using KEGG, GO, Progeny, GSVA, and GSEA. Results revealed significant variances in various immune-related pathways between high and low-risk cohorts. Analysis of the immune microenvironment using ssGSEA and ESTIMATE indicated that individuals with unfavorable prognoses had lower immune scores, stromal scores, and ESTIMATE scores, coupled with higher tumor purity. This suggests that high-risk individuals have compromised immune microenvironments, potentially contributing to their unfavorable prognoses. Additionally, drug sensitivity and molecular docking analysis revealed increased responsiveness to paclitaxel in high-risk individuals, implying its prognostic value. The JTB-encoded protein exhibited a negative binding energy of − 5.5 kcal/mol when interacting with paclitaxel, indicating its potential to enhance the patient's immune microenvironment. This framework enables patient prognosis prediction and sheds light on paclitaxel's mechanism in osteosarcoma treatment, facilitating personalized treatment approaches.**

**Keywords** Osteosarcoma, Centrosome, Tumor immune microenvironment, Prognostic model, Individualized therapy

Osteosarcoma is a malignant neoplasm that originates in the bone or soft tissues of the musculoskeletal system, including muscle, adipose, and connective tissues[1]. Although it predominantly affects adolescents and young adults, cases have been reported across all age groups[2]. The clinical presentation typically includes localized swelling, progressive bone pain, and pathological fractures[3]. The current standard of care for osteosarcoma is a multimodal approach integrating surgical resection, chemotherapy, and, in select cases, radiotherapy. Treatment strategies are tailored based on tumor size, anatomical location, histological characteristics, and the patient's overall health status[4]. Surgical excision remains the cornerstone of management, aiming for complete tumor

[1]Department of Orthopedics, Renmin Hospital of Wuhan University, No. 99 Zhangzhidong Road, Wuchang District, Wuhan 430060, China. [2]Department of Orthopedics Trauma, Hainan General Hospital (Hainan Affiliated Hospital of Hainan Medical University), Haikou 570311, Hainan, China. [3]Department of Orthopedics Trauma and Hand Surgery, The First Affiliated Hospital of Guangxi Medical University, Nanning 530021, Guangxi, China. [4]Department of Orthopedics, The Second Affiliated Hospital of Guangxi Medical University, Nanning 530007, Guangxi, China. [5]Yujian Zhong, Bohua Gao and Kai Tong contributed equally to this work. ✉email: weiqingjun@gxmu.edu.cn; hyrm2017@126.com

removal with negative margins. Neoadjuvant and adjuvant chemotherapy significantly reduce recurrence risk and improve overall survival by targeting micrometastatic disease. Radiotherapy, though less commonly employed, may be beneficial in cases where complete surgical resection is unfeasible or for local control of residual disease[5]. Recent advancements in molecular oncology have led to the integration of targeted therapies and immunotherapeutic approaches in osteosarcoma management. Targeted agents aim to disrupt key oncogenic pathways, while immunotherapies, including immune checkpoint inhibitors and adoptive T-cell therapies, hold promise in enhancing anti-tumor immune responses[6]. Despite these innovations, osteosarcoma prognosis remains highly variable, influenced by factors such as tumor stage at diagnosis, histological grade, presence of metastases, and response to therapy[7]. Early detection and timely intervention are critical in improving clinical outcomes. Patients diagnosed at an early stage and receiving prompt treatment achieve a 5-year survival rate exceeding 70%, whereas delayed diagnosis and advanced disease presentation correlate with significantly poorer prognoses[8]. Continued research into novel therapeutic targets and precision medicine approaches is essential to improving survival rates and quality of life for patients with osteosarcoma.

The centrosome is a cellular organelle composed of multiple proteins and RNA, located at the center of the nucleus, and plays a critical role in various biological processes, including gene expression, RNA processing, and cell cycle regulation[9]. In recent years, a growing body of research has highlighted the significant involvement of the centrosome in cancer initiation and progression[10]. Various aspects of the centrosome, such as its number, size, shape, and composition, exhibit distinct alterations in numerous cancer cells[10]. Concurrently, several centrosome-associated proteins and RNA molecules have been found to undergo abnormal expression or mutations in cancer, underscoring the centrosome's pivotal role in regulating cancer cell proliferation, metastasis, drug resistance, and immune evasion[11]. As a result, the centrosome has emerged as a promising target for cancer therapy, prompting the development of novel therapeutic strategies aimed at centrosome-specific interventions. Approaches such as siRNA, antibodies, and small-molecule compounds targeting centrosome-related proteins and RNA have been explored in cancer treatment, yielding promising preliminary findings[12]. Additionally, the expression of certain centrosome proteins has been identified as a potential prognostic biomarker, facilitating the assessment of treatment response and overall prognosis in cancer patients[13].

The immune microenvironment comprises various components surrounding a tumor, including tumor cells, immune cells, endothelial cells, fibroblasts, and a range of signaling molecules and pathways[14]. These components interact dynamically, collectively influencing tumor growth, metastasis, and treatment response. The therapeutic strategy of harnessing immune cells and immune-related molecules—such as immune checkpoint inhibitors, CAR-T cell therapy, and tumor vaccines—is known as immunotherapy[15]. In recent years, tumor research has increasingly focused on the immune microenvironment and immunotherapy. On one hand, accumulating evidence suggests that the immune microenvironment plays a crucial role in tumor initiation, progression, and response to therapy. By modulating the composition and function of the immune microenvironment, tumor cells can evade immune surveillance, ultimately leading to immune therapy resistance[16]. On the other hand, immunotherapy has demonstrated remarkable efficacy in certain tumor types, including melanoma, lung cancer, and breast cancer[17–19]. Moreover, growing evidence indicates that the effectiveness of immunotherapy is closely associated with the state of the immune microenvironment[20]. In some tumor types, therapeutic response is linked to the degree of immune cell infiltration. Therefore, investigating the relationship between the immune microenvironment and immunotherapy is essential for developing more effective tumor treatment strategies.

However, there remains a paucity of literature elucidating the significance and impact of the centrosome on the prognosis and immune microenvironment of osteosarcoma. This study aims to investigate the role of centrosome-associated genes in osteosarcoma. Furthermore, we developed a novel predictive model leveraging these findings to identify potential biomarkers and therapeutic targets for personalized immunotherapy. This approach is expected to enhance prognostic assessment and provide valuable guidance for clinical decision-making in osteosarcoma treatment.

## Materials and methods

### Data acquisition and preprocessing

We obtained RNA sequencing (RNA-seq) data from 88 individuals diagnosed with osteosarcoma through the TARGET initiative, retrieved from the UCSC XENA database. The raw data was originally provided in $\log_2$(FPKM + 1) format, but we converted it to $\log_2$ (TPM + 1) to achieve a more accurate assessment of gene expression levels. TPM (Transcripts Per Million) normalization accounts for variations in sequencing depth and gene length, making it more suitable than FPKM (Fragments Per Kilobase of transcript per Million mapped reads) for cross-sample comparisons of gene expression. This transformation enhances the comparability of our dataset with external validation cohorts and strengthens the robustness of downstream analyses. Among the 88 samples, 85 had complete survival and clinical information. To externally validate our findings, we obtained three additional osteosarcoma datasets (GSE16091, GSE21257, and GSE39055) from the Gene Expression Omnibus (GEO) database. These datasets were harmonized by removing batch effects before being used as independent validation cohorts.Additionally, we curated a set of 726 centrosome-associated genes (CTRGs) based on previous literature[21], of which 690 had available expression data for subsequent analysis.

### Constructing and evaluating a prognostic signature based on CTRGs

By integrating transcriptomic and survival data from the TARGET database, we randomly partitioned the samples into a training set and a test set at a 7:3 ratio. To further assess the robustness of our model, we incorporated independent osteosarcoma datasets from the GEO database (GSE16091, GSE21257, and GSE39055) as external validation cohorts. Initially, we performed a univariate Cox regression analysis to identify centrosome-associated genes (CTRGs) significantly associated with prognosis. Next, we applied least absolute shrinkage and selection operator (LASSO) regression to eliminate collinearity among these genes, followed by multivariate Cox

regression analysis to construct a prognostic model. These analyses were conducted using the glmnet package in R. The resulting model enables prognostic assessment by calculating the centrosome-related model score (CRMS) for each sample, computed using the following formula:

$$CRMS = \sum_{i=1}^{n} regression\ coefficient\ of\ gene\ i \times\ expression\ of\ gene\ i$$

To evaluate the predictive accuracy of the model, we performed receiver operating characteristic (ROC) curve analysis using the survivalROC package in R, assessing performance across both the internal test set and the external validation cohorts. Finally, we stratified patients into two risk groups based on their CRMS: the high-risk group (HR-group) and the low-risk group (LR-group).

### Development of a nomogram for predicting overall survival

A nomogram was constructed using the rms package in R to predict the overall survival of osteosarcoma (OS) patients. The model incorporated key clinical variables, including age, sex, metastasis status, and risk score. To evaluate the predictive accuracy of the nomogram, time-dependent calibration curves were generated, assessing its performance in estimating survival probabilities over time.

### Functional analysis of differentially expressed CTRGs

We performed differential gene expression analysis between the HR-group and LR-group using the limma package in R. Genes were considered differentially expressed if they met the criteria of $|\log FC| > 1$ and $FDR < 0.05$. To investigate protein-protein interaction (PPI) networks, we input the differentially expressed centrosome-associated genes (CTRGs) into the STRING database. The resulting PPI networks were then visualized using Cytoscape. Subsequently, we conducted functional enrichment analysis using Kyoto Encyclopedia of Genes and Genomes (KEGG)[22–24] and Gene Ontology (GO) to explore the biological pathways associated with the differentially expressed genes. The results were filtered using an FDR threshold of 0.05 and visualized using the enrichplot and ggplot2 packages in R.

### Construction of a protein–protein interaction (PPI) network

To investigate the interactions among differentially expressed genes (DEGs), we constructed a protein–protein interaction (PPI) network using the STRING database. The confidence score threshold was set to 0.4 to ensure reliable interactions. The resulting PPI network was then visualized using Cytoscape software for further analysis. To identify key regulatory genes, we employed the cytoHubba plugin and utilized the Maximal Clique Centrality (MCC) algorithm to rank genes based on their topological importance within the network. Genes with the highest MCC scores were considered potential hub genes, playing crucial roles in osteosarcoma progression. Additionally, we performed network topology analysis, assessing parameters such as degree centrality, betweenness centrality, and closeness centrality, to further characterize the functional significance of key genes within the network. This comprehensive analysis allowed us to identify critical genes that may serve as potential biomarkers or therapeutic targets for osteosarcoma.

### GSVA and GSEA analysis

We obtained standardized gene sets in KEGG and GO GMT format from the MsigDB database and utilized them for Gene Set Variation Analysis (GSVA) and Gene Set Enrichment Analysis (GSEA). For GSVA, we used the expression data of individual genes across samples as input to assess pathway enrichment status. Only pathways with a P-value < 0.05 were retained for further analysis. For GSEA, genes were ranked in descending order based on their logFC values before performing the analysis. Similarly, we retained only enriched pathways with a P-value < 0.05. Additionally, we employed the Progeny software to compute scores for 14 well-established cancer-associated pathways in the samples and examined their differences between the HR and LR cohorts.

### Evaluating immune infiltration and characterizing the immune microenvironment

To comprehensively assess the immune microenvironment of the samples, we employed multiple analytical approaches. First, we applied single-sample Gene Set Enrichment Analysis (ssGSEA) to quantify immune infiltration levels based on a set of 29 immune-related gene sets curated from previous literature. Next, we conducted Spearman correlation analysis to evaluate the relationships between target gene expression, risk scores, and immune-related scores. Subsequently, we utilized the ESTIMATE algorithm to systematically assess the immune and stromal components of the tumor microenvironment. Finally, we compared immune microenvironment differences between the HR-group and LR-group and visualized the results for further interpretation.

### Drug response analysis

To evaluate drug efficacy and identify potential therapeutic targets, we conducted a drug sensitivity analysis on 198 compounds using the oncoPredict package in R. We then calculated the half-maximal inhibitory concentration (IC50) values for each drug and compared the IC50 distributions between the HR-group and LR-group. To prioritize potential therapeutic candidates, we selected drugs with an average IC50 value below 1 for further investigation.

### Molecular docking and molecular dynamics simulation

The Protein Data Bank (PDB) (https://www.rcsb.org/) was used to obtain the 3D structure of proteins encoded by the model genes. To prepare the protein structures for molecular docking, we used PyMOL to remove water

molecules and organic ligands. The 2D structure of drug molecules was retrieved from the PubChem database (https://pubchem.ncbi.nlm.nih.gov/).Subsequently, AutoDock software was employed to assess the binding affinity and predict potential binding sites between drug compounds and target proteins. This analysis aimed to explore their molecular interactions and assess the feasibility of drug-protein binding.

### Culturing of human osteosarcoma cell line

The 143B osteosarcoma cell line was obtained from Wuhan Procell Life Science and Technology Co., Ltd. (Wuhan, China). The cells were cultured in Dulbecco's Modified Eagle Medium (DMEM) supplemented with 10% fetal bovine serum (FBS) and 1% penicillin–streptomycin. The cultures were maintained in a humidified incubator at 37 °C with 5% $CO_2$ to ensure optimal growth conditions.

### Gene silencing

SiRNA targeting the JTB gene and control siRNA were acquired from Beijing Tsingke Biotech Co., Ltd. The 143B cell line was seeded in a 6-well plate and subsequently transfected with siRNA using Lipofectamine 2000. Following the attainment of cell confluency, they were utilized for subsequent experiments. The siRNA sequence used to knock down JTB gene expression is as follows: Sense strand: GGAAGAGUUUGUGGUAGCA, Antisense strand: UGCUACCACAAACUCUUCC. The knockdown efficiency was assessed using qRT-PCR.

### qRT-PCR

TRIzol reagent was used to extract the entire RNA from osteosarcoma cells, followed by reverse transcription using the TransScript First-Stand cDNA Synthesis Kit (TaKaRa, Japan). qRT-PCR was carried out on an ABI-7900HT Real-Time PCR System using SYBR Green MasterMix (TaKaRa, Japan). The primer sequences were as follows: GAPDH forward: 5′-CGCTCTCTGCTCCTCCTGT-3′; reverse: 5′-ATCCGTTGACTCCGACCTA-3′. JTB forward: 5′-AATAGGCAACTCCGGCCTTC-3′; reverse: 5′-AGAGGGACCTACTCCACAGG-3′.

### CCK-8 assay

Cells transfected with siRNA were seeded into 96-well plates at a density of 5000 cells per well. Once the cells adhered and stabilized, the original medium was removed, and the wells were washed with PBS. Subsequently, 100 µL of fresh medium containing 10 µL of CCK-8 reagent was added to each well, followed by incubation at 37 °C. After 1 h, the absorbance at 450 nm was measured using a microplate reader. Cell viability was calculated using the following formula:

$$\begin{aligned}&\text{Cell viability}\ (\%)\\&= [(\text{OD value of experimental well} - \text{OD value of blank well}) / (\text{OD value of control well} - \text{OD value of blank well})] \times 100\%.\end{aligned}$$

### EdU assay

The EdU assay was performed to assess cell proliferation. After siRNA treatment, cells were seeded onto glass slides and allowed to adhere. Staining was carried out using the EdU Kit (Beyotime) according to the manufacturer's instructions. Following incubation, the medium containing EdU was removed, and cells were fixed with paraformaldehyde. After permeabilization, DAPI staining was applied to visualize the nuclei. The stained cells were then observed and imaged using an upright fluorescence microscope.

### Cell apoptosis detection

After treatment, 143B cells were harvested for apoptosis detection. The culture medium was first transferred to a new centrifuge tube to retain any detached cells. The adherent cells were then washed with PBS, and the remaining medium was removed. A total of 100,000 to 500,000 suspended cells were collected and centrifuged at 300 × g for 5 min. The cell pellet was resuspended in 500 µL of Annexin V-binding buffer. Subsequently, 5 µL of Annexin V and 5 µL of nuclear staining solution were added to the suspension. The mixture was gently vortexed and incubated at room temperature for 15–20 min in the dark. Finally, flow cytometry was performed to assess apoptosis.

### Would healing assay

The 143B osteosarcoma cell line was cultured in 6-well plates and treated with si-JTB or si-NC. Once the cells reached confluence, a uniform scratch was introduced using a micropipette tip to simulate a wound. The medium was then replaced with serum-free DMEM to prevent cell proliferation from influencing migration results. Microscopic images of the wound area were captured at 0 h, 24 h, and 48 h post-wounding to assess cell migration. The wound area was quantified using ImageJ software, and the percentage of wound closure was calculated at 24 h and 48 h using the following formula:

$$\text{Would healing percentage} = (\text{area of } 0\,\text{h} - -\text{area of } 24\,\text{h or } 48\,\text{h}) / (\text{area of } 0\,\text{h})$$

### Transwell migration assay

Following treatment, 40,000 cells suspended in serum-free medium were seeded into the upper chamber of a Transwell insert pre-coated with Matrigel. The lower chamber was filled with medium containing 10% fetal bovine serum (FBS) to serve as a chemoattractant. After 24 h of incubation, cells that migrated through the membrane were fixed with pre-cooled formaldehyde and subsequently stained with crystal violet. The stained cells were then imaged and quantified using an Olympus microscope (Japan).

### Colony formation assay

The colony formation assay was performed to evaluate the clonogenic potential of cells. siRNA-treated cells were seeded into 6-well plates at a low density (~ 500 cells per well) and cultured for 10–14 days until visible colonies had formed. The culture medium was refreshed every 3 days. After the incubation period, the colonies were fixed with 4% paraformaldehyde for 15 min and subsequently stained with 0.1% crystal violet for 30 min. The number of colonies was then counted and photographed to assess cell proliferation capacity.

### In vivo experiments

Four-week-old male BALB/c nude mice were purchased from Beijing Huafukang Laboratory Animal Center (Beijing, China) and housed at the Animal Center of Renmin Hospital of Wuhan University. Following acclimatization, $5 \times 10^6$ control or siRNA-treated 143B cells were subcutaneously implanted into the mice. Tumor volume was measured every 5 days as previously described. On day 25 post-injection, all mice were anesthetized with isoflurane and euthanized using $CO_2$ overdose. Tumors were subsequently excised and weighed. All animal care and experimental procedures were conducted in accordance with the ethical guidelines and approved protocols of the Animal Ethics Committee of Renmin Hospital of Wuhan University.

### Statistical analysis

The Wilcoxon rank-sum test is employed to assess if there exists a notable distinction between two groups, whereas the Kruskal–Wallis test is employed to assess if there exists a notable distinction among a minimum of three groups of data. The statistical analysis was performed using version 4.2.0 of the R package. Statistically significant results were considered for all analysis with a significance level of less than 0.05.The symbol "*" indicated a significance level of $p < 0.05$, "**" indicated a significance level of $p < 0.01$, and "***" indicated a significance level of $p < 0.001$.

## Results

### Development of a centrosome-related prognostic model

Among the 690 centrosome-related genes (CTRGs), we identified 67 genes significantly associated with prognosis through univariate Cox regression analysis (Supplementary Table S1). To refine the model and minimize redundancy, we applied LASSO regression analysis (Fig. 1A,B), ultimately selecting five key genes: SPICE1 (Spindle and Centriole Associated Protein 1), HOOK2 (Hook Microtubule Tethering Protein 2), GNAI2 (G Protein Subunit Alpha I2), JTB (Jumping Translocation Breakpoint), and RPS27 (Ribosomal Protein S27). These genes were further validated through multivariate Cox regression analysis, confirming their independent prognostic significance (Fig. 1C). To quantify prognostic risk, we formulated the Centrosome-Related Model Score (CRMS). Using the median CRMS value in the training cohort as a threshold, we stratified patients into a high-risk group (HR-group) and a low-risk group (LR-group). In the training set, 30 patients were assigned to each group, and Kaplan-Meier survival analysis demonstrated that the HR-group exhibited significantly poorer overall survival (OS) compared to the LR-group (Fig. 2A). The same classification approach was applied to the test set and the external validation cohort (GEO database), both of which exhibited a consistent trend, underscoring the robustness of our model (Fig. 2A). To assess the predictive accuracy of CRMS, we conducted receiver operating characteristic (ROC) curve analysis at 1, 3, and 5 years using the survivalROC package. The area under the curve (AUC) values were: Training set: 0.850, 0.941, and 0.96, Test set: 0.739, 0.625, and 0.770 ,GEO validation cohort: 0.867, 0.751, and 0.795. These results indicate that CRMS is a reliable predictor of patient prognosis (Fig. 2B). Heatmap visualization of gene expression patterns revealed that SPICE1, HOOK2, JTB, and RPS27 were upregulated in the HR-group, whereas GNAI2 was downregulated, consistent with their risk profiles (Fig. 2C). Further survival analyses identified CRMS and metastasis as significant factors influencing OS in univariate Cox regression analysis (Table 1), and multivariate Cox regression confirmed their status as independent prognostic factors (Table 2). Finally, time-dependent ROC curve analysis demonstrated that CRMS outperformed other clinical variables in predicting patient survival (Fig. 3A,B), reinforcing its clinical utility. These findings collectively indicate that we have successfully developed a robust centrosome-related prognostic model for osteosarcoma, which may facilitate risk stratification and personalized treatment strategies.

### Development of a nomogram for survival prediction

A nomogram was developed by integrating age, sex, and metastasis status into a predictive model to estimate the overall survival (OS) of osteosarcoma patients (Fig. 3C). To assess the predictive performance of the nomogram, calibration curves were generated at 1, 3, and 5 years, demonstrating a high degree of alignment between the predicted and observed survival outcomes (Fig. 3D). These findings suggest that our nomogram serves as a highly effective clinical tool for assessing survival probability and providing prognostic insights for individuals diagnosed with osteosarcoma.

### Differentially expressed genes (DEGs) and functional assessment in risk groups

After stratifying patients into high-risk and low-risk groups, we conducted a differential expression analysis based on the criteria outlined in the Methods section, identifying a total of 67 differentially expressed genes (DEGs) (Fig. 4A,B). To further explore the biological significance of these DEGs, we constructed a protein-protein interaction (PPI) network using the STRING database, which revealed extensive interconnections among the DEGs, suggesting their potential involvement in shared biological pathways (Fig. 4C). To identify key regulatory genes within the network, we employed the Maximal Clique Centrality (MCC) algorithm in CytoHubba, ranking genes based on their centrality in the interaction network. The top-ranked genes, considered pivotal regulators influencing clinical divergence between risk groups, are detailed in Supplement Table S2 (Fig. 4D). To further elucidate the functional implications of these DEGs, we performed Gene Ontology (GO) and Kyoto Encyclopedia

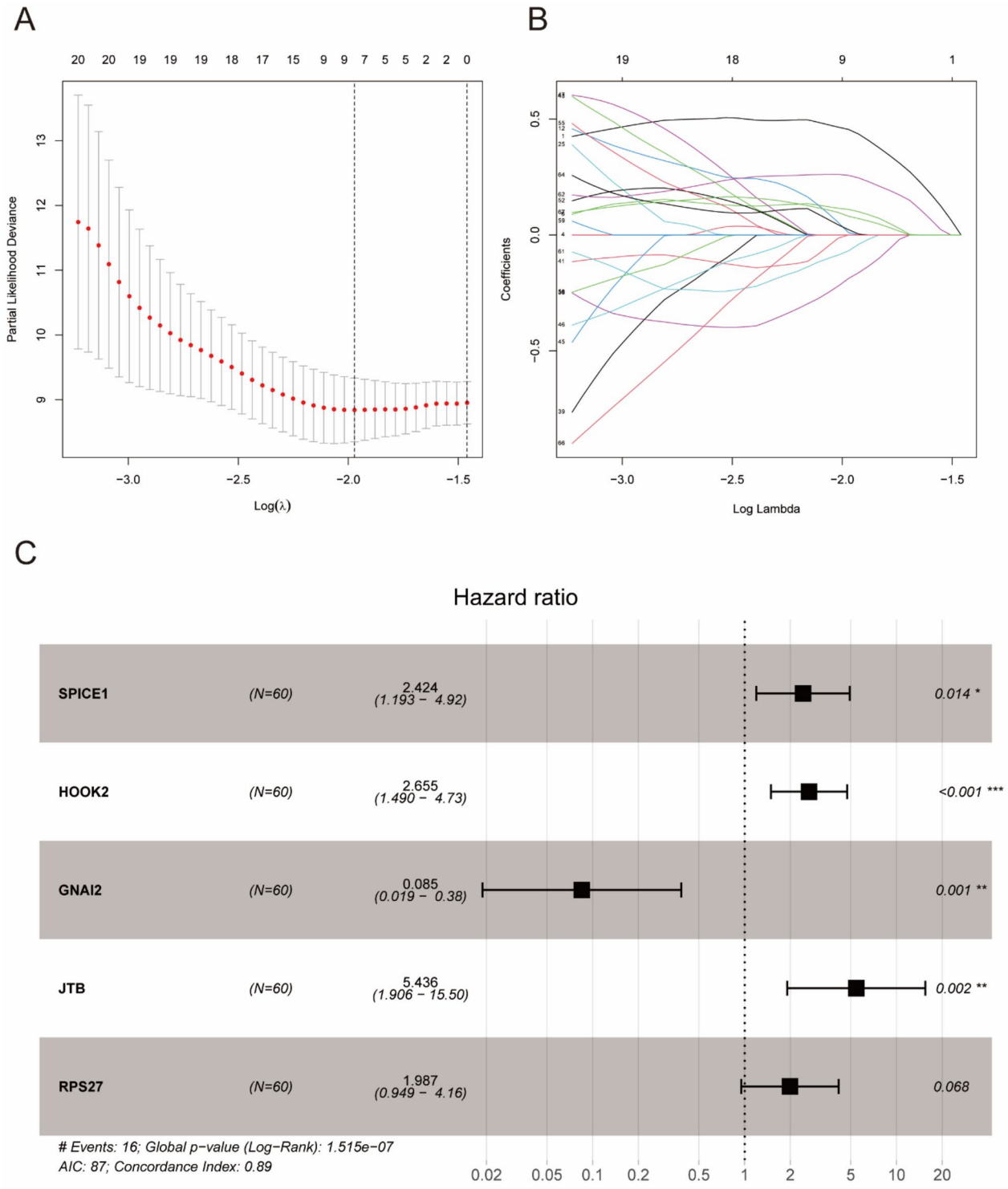


**Fig. 1**. Constructing a prognostic model based on CTRGs. (**A**) Selection of the optimal tuning parameter (λ) in the LASSO Cox regression model using tenfold cross-validation. The vertical dashed line represents the optimal λ value, which minimizes the partial likelihood deviance. (**B**) LASSO coefficient profiles of the candidate genes. As the tuning parameter λ increases, coefficients shrink toward zero, with the final selected genes identified at the optimal λ. (**C**) Forest plot displaying the hazard ratios (HR) and 95% confidence intervals (CI) of the five CTRGs (SPICE1, HOOK2, GNAI2, JTB, RPS27) in the multivariate Cox regression analysis. The HR values indicate the association of each gene with osteosarcoma prognosis, with SPICE1, HOOK2, JTB, and RPS27 identified as risk factors and GNAI2 as a protective factor. The global p-value for the model is 1.515e-07, with an Akaike Information Criterion (AIC) of 87 and a concordance index (C-index) of 0.89, indicating strong predictive performance.

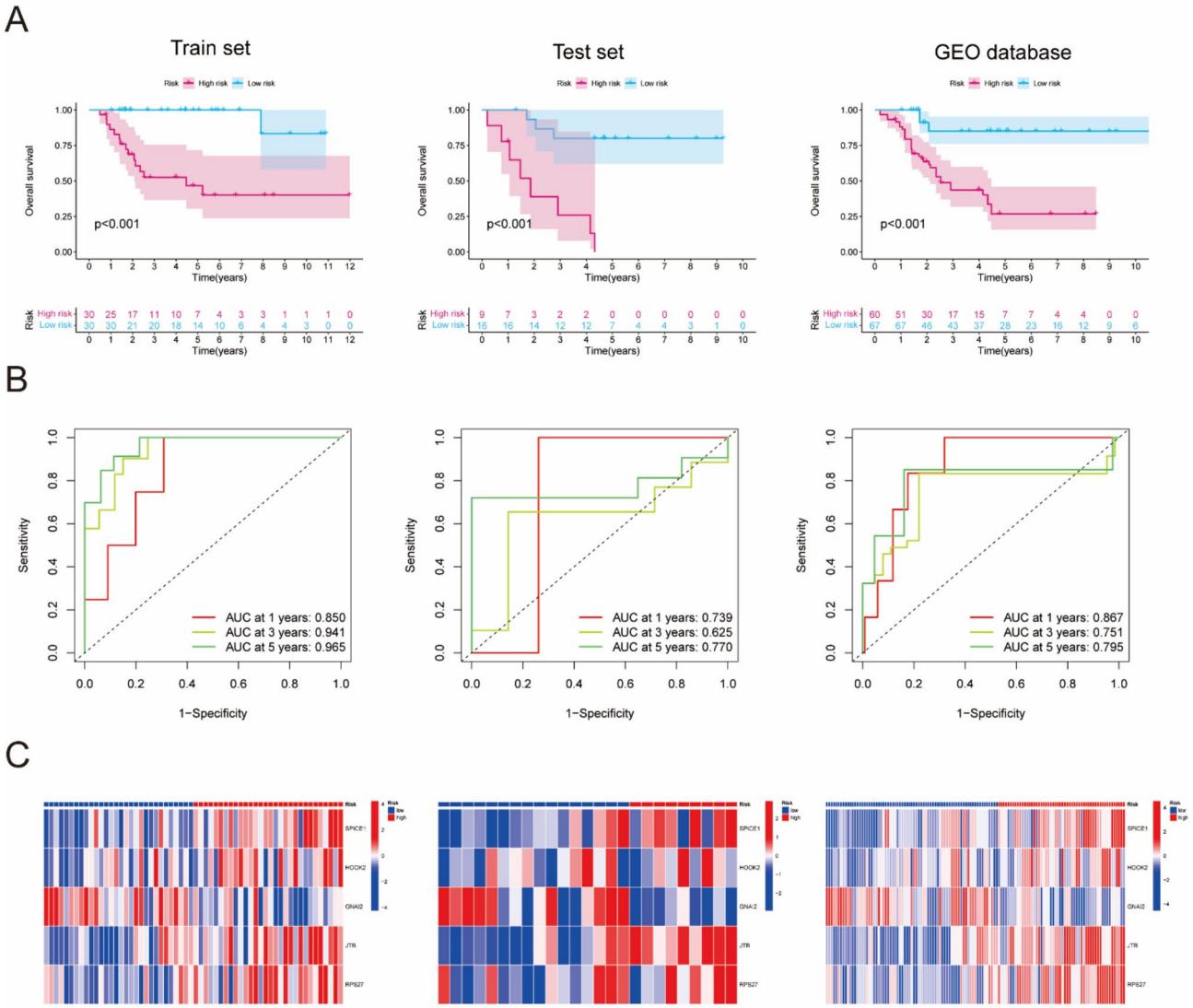


**Fig. 2**. Validation of the prognostic model based on CTRGs. (**A**) Kaplan–Meier survival analysis of osteosarcoma patients in the training set, test set, and GEO validation cohort. Patients were stratified into high-risk (HR) and low-risk (LR) groups based on the prognostic model. In all three datasets, patients in the HR-group exhibited significantly poorer survival compared to those in the LR-group ($p < 0.001$). (**B**) Receiver operating characteristic (ROC) curves assessing the predictive performance of the model at 1, 3, and 5 years in the training set (left), test set (middle), and GEO validation cohort (right). The area under the curve (AUC) values indicate strong prognostic ability, with the external GEO validation set achieving an AUC of 0.795 for 5-year survival. (**C**) Heatmaps illustrating the expression patterns of the five prognostic genes (SPICE1, HOOK2, GNAI2, JTB, RPS27) in the training, test, and GEO validation cohorts. SPICE1, HOOK2, JTB, and RPS27 are highly expressed in the HR-group, while GNAI2 is downregulated in the HR-group across all datasets.

| Id | HR | HR.95 L | HR.95 H | *p* value |
|---|---|---|---|---|
| Gender | 0.589957 | 0.220102 | 1.581308 | 0.294171 |
| Age | 0.999822 | 0.999488 | 1.000157 | 0.296933 |
| Metastasis | 6.165921 | 2.27241 | 16.73051 | 0.000355 |
| Riskscore | 1.02179 | 1.01114 | 1.032552 | 5.52E−05 |

**Table 1**. Univariate analysis of clinical parameters.

| Id | HR | HR.95 L | HR.95 H | *p* value |
|---|---|---|---|---|
| Gender | 0.812697 | 0.254226 | 2.597982 | 0.726503 |
| Age | 0.999845 | 0.999402 | 1.000289 | 0.494573 |
| Metastasis | 4.151228 | 1.374424 | 12.53812 | 0.011607 |
| Riskscore | 1.018611 | 1.007414 | 1.029932 | 0.001076 |

**Table 2**. Multivariate analysis of clinical parameters.

of Genes and Genomes (KEGG) enrichment analyses. GO analysis revealed significant enrichment in immune-related biological processes, including neutrophil activation, myeloid leukocyte activation, and macrophage chemotaxis, indicating that immune activity may serve as a crucial factor distinguishing high-risk from low-risk patients (Fig. 4F). KEGG pathway analysis identified 12 significantly enriched pathways, such as complement and coagulation cascades, osteoclast differentiation, phagosome formation, and acute myeloid leukemia, further supporting the involvement of immune-related processes in osteosarcoma prognosis (Fig. 4E). These findings collectively indicate that variations in immune-associated signaling pathways and biological processes contribute to differences in prognosis between the two risk groups, suggesting that immune dysregulation plays a critical role in osteosarcoma progression.

## GSVA analysis

Using Gene Set Variation Analysis (GSVA), we evaluated pathway and biological process activity for each sample and analyzed differences in pathway scores between the high-risk and low-risk groups. Gene sets from both the KEGG and GO databases were examined, revealing 36 significantly altered pathways in KEGG and 1216 in GO. For visualization, we presented the top 20 most significant pathways from each analysis. In the KEGG results, key immune-related pathways, including leukocyte transendothelial migration, complement and coagulation cascades, cell adhesion molecules (CAMs), and natural killer cell-mediated cytotoxicity, were notably downregulated in the high-risk group (HR-group), indicating a compromised immune environment (Fig. 5A). Consistent findings were observed in the GO database, where the most significantly altered biological processes were predominantly immune-related and exhibited marked downregulation in the HR-group (Fig. 5B). To further explore pathway alterations, we employed the Progeny package to assess 14 classic tumor-associated signaling pathways. The results revealed significant differences in EGFR, JAK-STAT, NFκB, TNFα, and TRAIL pathways, all of which demonstrated decreased activity in the HR-group (Fig. 5C). Additionally, we investigated the relationships between risk scores, JTB expression levels, and the five tumor-related pathways, revealing that higher risk scores were significantly correlated with lower activity in these pathways (Fig. 5D–H). However, when examining the correlation between JTB expression and pathway activity, we found that only the TRAIL pathway exhibited a significant inverse correlation with JTB expression (Fig. 5I–M). These findings suggest substantial immune function differences between the high-risk and low-risk groups, as identified by the centrosome-related prognostic model. Moreover, individuals in the high-risk group exhibit significantly impaired immune function, further reinforcing the potential link between centrosome-related gene dysregulation and immune suppression in osteosarcoma.

## GSEA analysis

The Gene Set Enrichment Analysis (GSEA) revealed that a majority of genes downregulated in the high-risk group (HR-group) were significantly enriched in immune-related pathways. Analysis using the KEGG standard gene set indicated that pathways such as antigen processing and presentation, B cell receptor signaling, chemokine signaling, and T cell receptor signaling were predominantly associated with the suppressed genes in the HR-group (Fig. 6A,B). Similarly, the GO standard gene set analysis demonstrated significant downregulation in key immune-associated processes, including adaptive immune response, antigen receptor-mediated signaling, and immune response-regulating signaling pathways (Fig. 6C,D). These findings suggest that immune dysfunction is a prominent feature of the HR-group, which may contribute to poor patient prognosis.

## Immune infiltration

Given the significant differences in immune function between the two risk groups, we conducted immune infiltration analyses using single-sample Gene Set Enrichment Analysis (ssGSEA) and ESTIMATE to further investigate disparities in the tumor immune microenvironment. The ssGSEA analysis revealed that 25 out of 29 immune-related gene sets exhibited significant differences between the high-risk (HR) and low-risk (LR) groups, with all of these sets displaying reduced scores in the HR-group (Fig. 7A,B). Correlation analysis further indicated a negative correlation between risk score, JTB expression levels, and immune function, suggesting that patients with higher risk scores and increased JTB expression may experience impaired immune function, potentially contributing to poor prognosis (Fig. 7C,D). To complement these findings, we employed ESTIMATE to compute an overall immune score for each sample. The results indicated that ESTIMATEScore, StromalScore, and ImmuneScore were significantly lower in the HR-group, while TumorPurity was markedly higher compared to the LR-group (Fig. 7E–H). Similarly, individuals with higher risk scores and elevated JTB expression exhibited lower ESTIMATE scores and higher tumor purity, further supporting the hypothesis of immune dysfunction in the HR-group (Fig. 7I–P). These findings suggest that dysregulation of the tumor immune microenvironment plays a key role in differential patient prognosis. The observed immune suppression in the HR-group highlights

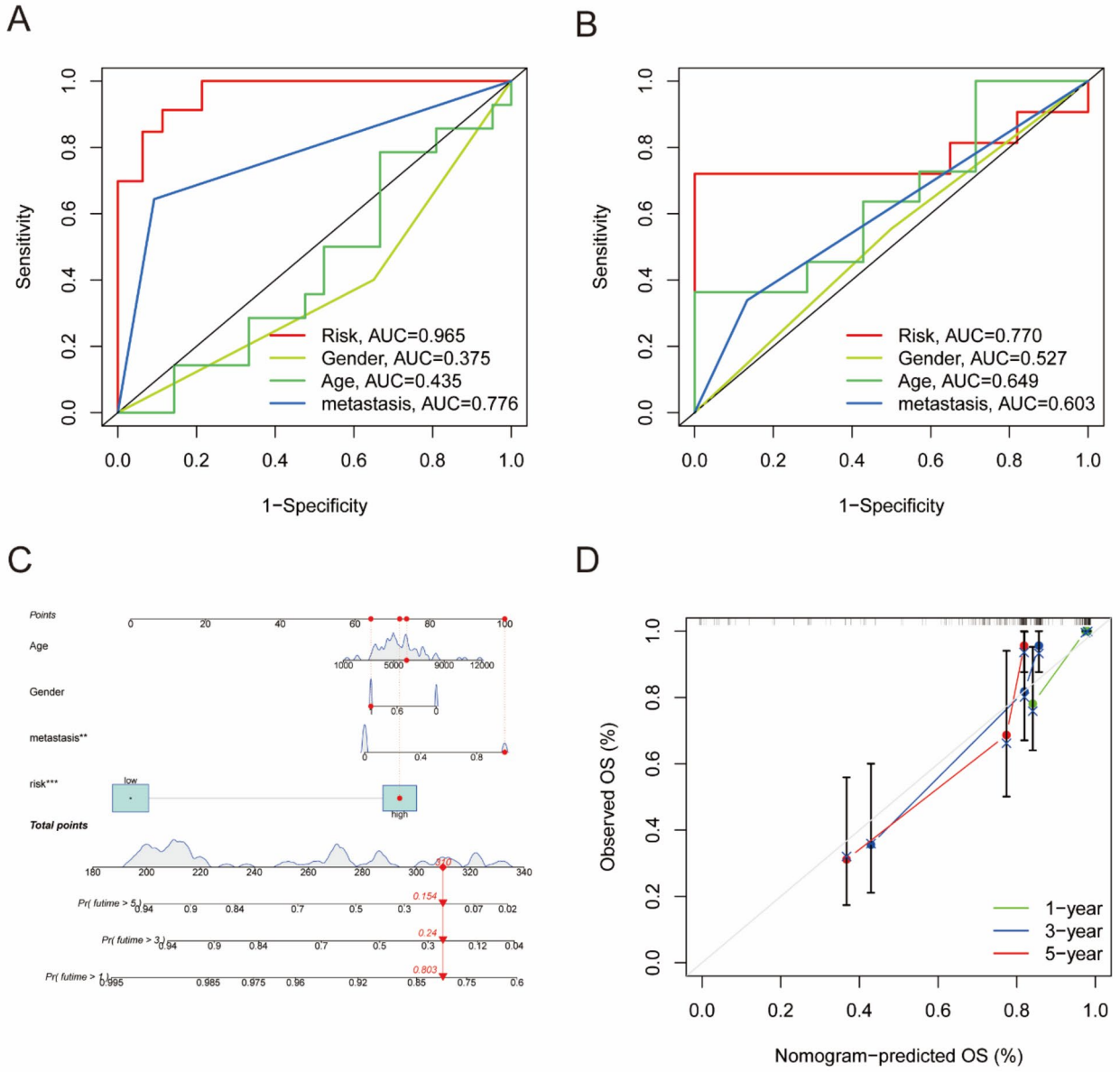


**Fig. 3**. Performance evaluation and clinical application of the prognostic model. (**A**,**B**) Receiver operating characteristic (ROC) curves comparing the prognostic model's performance with clinical factors (gender, age, and metastasis status) in the training set (**A**) and test set (**B**). The risk score-based model exhibits superior predictive performance, with an AUC of 0.965 in the training set and 0.770 in the test set, outperforming other clinical variables. (**C**) Nomogram integrating the prognostic model with clinical variables (age, gender, metastasis status, and risk score) to predict 1-year, 3-year, and 5-year overall survival (OS) in osteosarcoma patients. The scoring system allows individualized survival probability estimation. (**D**) Calibration curves assessing the agreement between predicted and observed OS probabilities at 1-year, 3-year, and 5-year time points. The nomogram predictions closely align with actual survival outcomes, demonstrating high predictive accuracy.

the potential for targeted therapeutic interventions aimed at restoring immune function, which could improve patient outcomes through immunomodulatory drugs or alternative strategies.

## Sensitivity to drugs

To assess drug responsiveness in osteosarcoma, we conducted drug sensitivity analysis on 198 different compounds and calculated the half-maximal inhibitory concentration (IC50) values for each drug. The results revealed significant differences in IC50 values for 31 drugs between the high-risk (HR) and low-risk (LR) groups (Fig. 8A). Since a higher IC50 value indicates lower drug sensitivity, we focused on drugs with an average

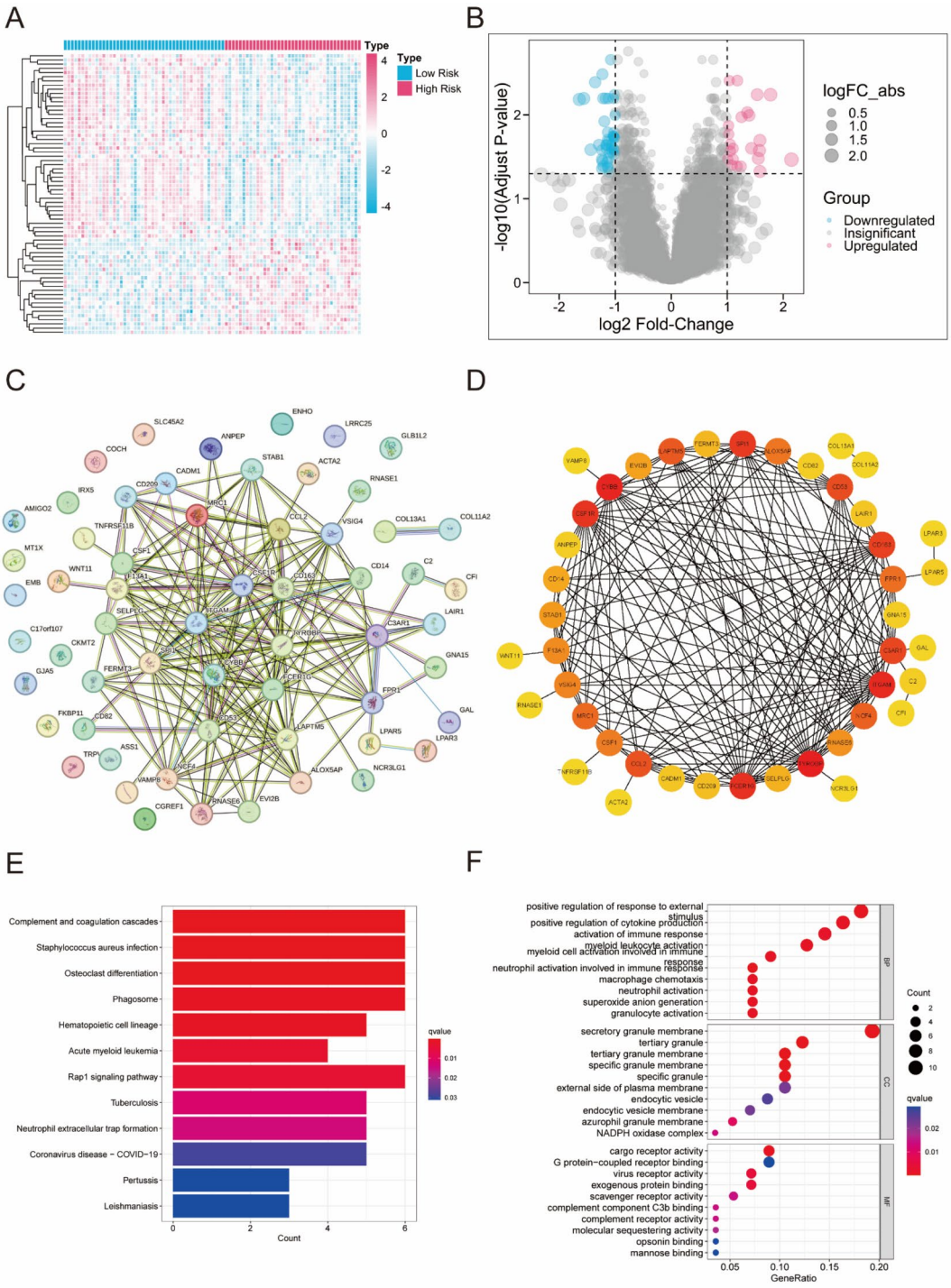


**Fig. 4**. Differential expression analysis, protein–protein interaction (PPI) network, and functional enrichment analysis of CTRGs. (**A**) Heatmap of differentially expressed genes (DEGs) between the high-risk (HR) and low-risk (LR) groups. Upregulated and downregulated genes are indicated in red and blue, respectively. (**B**) Volcano plot displaying the distribution of DEGs. Upregulated genes are highlighted in pink, downregulated genes in blue, and non-significant genes in gray. The x-axis represents the log2 fold change, while the y-axis represents the – log10 adjusted p-value. (**C**) Protein–protein interaction (PPI) network of DEGs constructed using STRING. Nodes represent proteins, and edges indicate predicted interactions. (**D**) Visualization of hub genes in the PPI network, ranked by degree of connectivity. Nodes are color-coded based on their centrality, with highly connected genes in red and less connected genes in yellow. (**E**) KEGG pathway enrichment analysis of DEGs, showing significantly enriched pathways related to immune response, infectious diseases, and cancer. (**F**) Gene Ontology (GO) enrichment analysis, including biological processes (BP), molecular functions (MF), and cellular components (CC), highlighting key immune and signaling pathways associated with osteosarcoma prognosis.

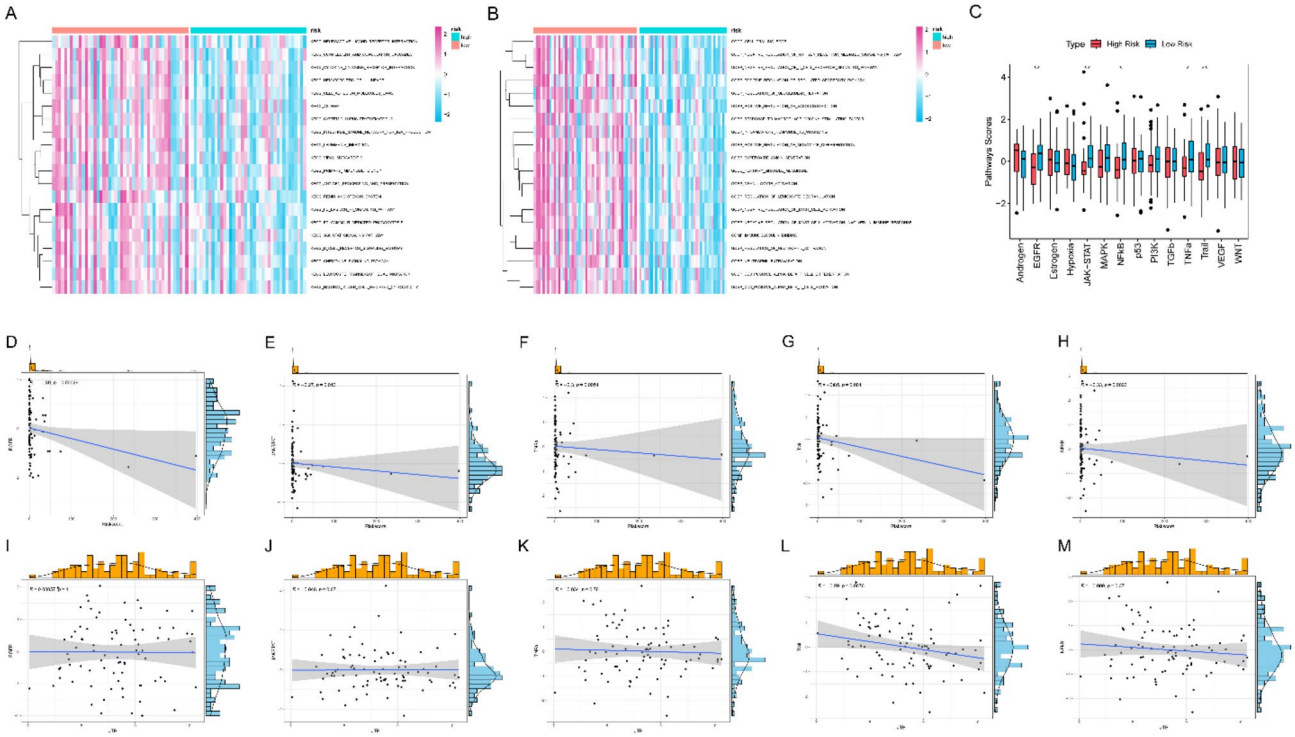


**Fig. 5**. GSVA-based functional enrichment analysis and correlation between the risk score, key pathways, and gene expression. (**A**,**B**) Heatmaps showing the enrichment levels of KEGG (**A**) and GO BP (**B**) pathways between the high-risk and low-risk groups based on Gene Set Variation Analysis (GSVA). The color gradient represents the relative pathway activity. (**C**) Boxplot comparing pathway scores between the high-risk and low-risk groups for multiple oncogenic and immune-related signaling pathways. Statistically significant differences are indicated (**$p < 0.05$, **$p < 0.01$). (**D**–**H**) Correlation analysis between the risk score and immune-related pathways, including EGFR, JAK-STAT, NF-κB, PI3K, and TGF-β signaling, derived from GSVA. Pearson correlation coefficients (R) and p-values are indicated in each panel. (**I**–**M**) Correlation analysis between JTB expression and key immune-related pathways identified through GSVA, demonstrating the potential involvement of JTB in osteosarcoma progression. Pearson correlation coefficients (R) and p-values are indicated.

IC50 value below 1, identifying Sepantronium bromide, Daporinad, Paclitaxel, and Sabutoclax as promising candidates (Fig. 8B–E). Among these four drugs, Paclitaxel exhibited the most notable predictive efficacy, with the HR-group demonstrating increased sensitivity to this drug, as indicated by its lower IC50 value. This suggests that Paclitaxel may provide greater therapeutic benefits for high-risk patients classified by our centrosome-based model. Further investigation into Paclitaxel's mechanism of action revealed a strong association with the centrosome, suggesting that it may exert its anticancer effects by interacting with genes identified in our model.

## Molecular docking

Building on our previous findings, we hypothesized a potential correlation between JTB and the anticancer effects of paclitaxel. To explore this, we conducted molecular docking analysis to examine their potential binding interactions. AutoDock analysis identified 20 potential interaction sites between paclitaxel and the protein encoded by JTB. For further investigation, we selected the binding conformation with the most negative binding free energy (− 5.5 kcal/mol), indicating a stable interaction (Fig. 8F). A detailed structural analysis of the interaction site revealed that paclitaxel binds to the JTB-encoded protein via hydrogen bonding, suggesting a potential regulatory effect (Fig. 8G). Based on this observation, we speculate that paclitaxel may exert its therapeutic effects by binding to and inactivating the JTB-encoded protein, thereby disrupting its function. This mechanism may contribute to enhancing immune responses while simultaneously reducing cancer cell activity and migration, offering new insights into the therapeutic potential of paclitaxel in osteosarcoma treatment.

## Knocking down JTB suppresses cell growth and enhances apoptosis in 143B

To assess the effects of si-JTB, we first validated JTB mRNA levels using qRT-PCR, which confirmed a significant reduction in JTB transcription following knockdown (Fig. 9A). To further investigate the functional impact of JTB suppression, we evaluated cell viability and proliferation in siRNA-treated 143B cells. The CCK-8 assay demonstrated that JTB knockdown led to partial growth arrest, indicating a reduction in cell viability (Fig. 9B). Consistently, EdU staining revealed a marked decrease in the percentage of EdU-positive cells, suggesting a significant inhibition of 143B cell proliferation upon JTB knockdown (Fig. 9C,D). Additionally, flow cytometry

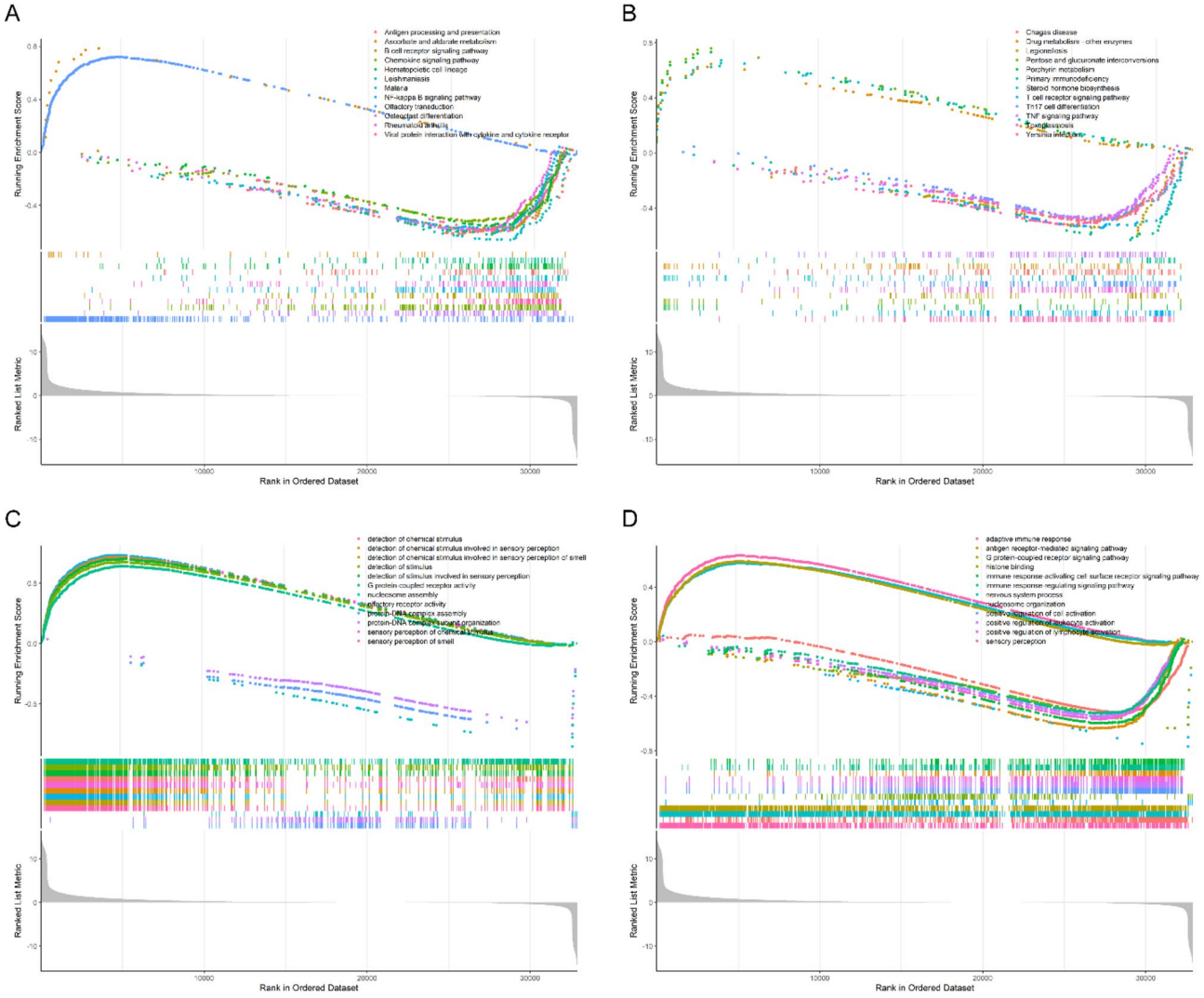


**Fig. 6**. GSEA-based enrichment analysis of pathways in high-risk and low-risk groups. (**A**,**B**) KEGG pathway enrichment analysis using Gene Set Enrichment Analysis (GSEA). The enrichment scores indicate pathway activity differences between high-risk and low-risk groups. (**A**) Enriched pathways in the high-risk group, including antigen processing and presentation, hematopoietic cell lineage, and cytokine receptor interactions. (**B**) Enriched pathways in the low-risk group, such as drug metabolism, tight junction signaling, and TGF-β signaling pathway. (**C**,**D**) GO biological process enrichment analysis based on GSEA. (**C**) Pathways enriched in the high-risk group, predominantly associated with sensory perception, G-protein coupled receptor activity, and stimulus detection. (**D**) Pathways enriched in the low-risk group, including immune response activation, positive regulation of cell activation, and adaptive immunity.

analysis showed that si-JTB induced apoptosis in 143B cells, further confirming its role in promoting programmed cell death (Fig. 9E,F). These findings collectively suggest that JTB is critical for 143B cell survival, as its inhibition directly suppresses cell growth and enhances apoptosis, reinforcing our previous analyses on its role in osteosarcoma pathogenesis.

## Knocking down JTB impairs colony formation, migration, and invasion, while suppressing tumor growth in vivo

To examine the effects of JTB knockdown on osteosarcoma cell behavior, we conducted a series of functional assays. Colony formation assays revealed that si-JTB significantly reduced the number of colonies compared to the control and si-NC groups, suggesting impaired proliferative capacity (Fig. 10A, B). Similarly, Transwell migration assays demonstrated a significant reduction in the number of migrating cells in the si-JTB group, indicating decreased migratory ability (Fig. 10C,D). To further assess the impact of JTB knockdown on cell migration, we performed scratch wound healing assays, capturing images at 24- and 48-h post-wounding. The si-JTB group exhibited significantly lower wound closure percentages than the control and si-NC groups, further confirming impaired migratory capacity (Fig. 10E–G). To evaluate the role of JTB in tumor progression, we utilized a xenograft mouse model. Tumors in the si-JTB group were visibly smaller than those in the control

and si-NC groups (Fig. 10H), with a significant reduction in tumor volume observed over time (Fig. 10I). Collectively, these findings demonstrate that JTB knockdown suppresses colony formation, migration, and invasion of 143B osteosarcoma cells in vitro and inhibits tumor growth in vivo, highlighting the critical role of JTB in osteosarcoma progression and its potential as a therapeutic target.

## Discussion

Osteosarcoma remains a significant factor affecting the healthy development of adolescents[25]. Despite its low incidence, its poor prognosis continues to pose a major clinical challenge. Current treatment strategies still rely heavily on early diagnosis, making the identification of novel biological markers and therapeutic targets crucial for improving patient outcomes[26]. The centrosome, a key cellular organelle in eukaryotic cells, has been implicated in various cancers[27]. However, its precise role and mechanism in osteosarcoma remain largely unexplored. In this study, we curated centrosome-related genes to construct a prognostic model for osteosarcoma patients and evaluated their survival outcomes using this model. Simultaneously, we conducted mechanistic analyses, immune microenvironment characterization, and drug sensitivity profiling to identify potential immunotherapy targets and viable therapeutic options. These findings provide clinicians with valuable insights for refining treatment strategies and monitoring disease progression, ultimately contributing to personalized osteosarcoma management.

By constructing a centrosome-related prognostic model, we identified five key model genes: GNAI2, SPICE1, RPS27, HOOK2, and JTB. GNAI2 (G protein subunit alpha i2) encodes an α-subunit of guanine nucleotide-binding proteins (G proteins), which plays a role in hormonal regulation of adenylate cyclase by binding guanine nucleotides. SPICE1 (spindle and centriole associated protein 1) is involved in metaphase plate congression, mitotic spindle assembly, and centriole replication regulation. RPS27 (ribosomal protein S27) encodes a C4-type zinc finger domain-containing protein, which may bind to zinc and nucleic acids, suggesting its role in ribosomal function. HOOK2 (hook microtubule anchoring protein 2) is a cytosolic coiled-coil protein that interacts with microtubules via its conserved N-terminal domain, while its C-terminal domain binds to organelles, facilitating intracellular trafficking. JTB (jumping translocation breakpoint) plays a role in mitotic cytokinesis and the regulation of protein kinase activity, localizing to the cytoplasm, midbody, centrosome, and spindle apparatus. By evaluating the expression profiles of these five genes, we stratified patients into high-risk (HR-group) and low-risk (LR-group) categories. Among these genes, JTB exhibited the highest hazard ratio (HR), suggesting a strong influence on disease progression and prognosis in osteosarcoma patients. Given that JTB's role in osteosarcoma remains unexplored, we focused subsequent investigations on elucidating its biological impact in this malignancy. To further validate the function of JTB, we conducted a series of experimental assays using osteosarcoma cell lines, aiming to clarify its mechanistic involvement in disease progression.

Next, we conducted functional enrichment analysis to compare the biological differences between the high-risk and low-risk groups, revealing significant disparities in immune function and associated biological mechanisms. Additionally, pathway scoring of conventional signaling pathways identified five pathways with significant differences, among which only the TRAIL pathway exhibited a notable association with JTB expression. The TRAIL pathway, also known as the TNF-related apoptosis-inducing ligand (TRAIL) pathway, plays a critical role in cellular apoptosis[28]. TRAIL, a ligand that induces programmed cell death, binds to its receptors, TRAIL-R1 (DR4) and TRAIL-R2 (DR5), on the cell surface, thereby triggering apoptotic signaling cascades[29]. This pathway is essential in regulating cancer cell survival and apoptosis, and its activation can inhibit tumor growth and metastasis[30]. Our findings suggest an inverse relationship between JTB expression and the TRAIL pathway, implying that elevated JTB levels may suppress TRAIL signaling, thereby enhancing tumor cell proliferation. Furthermore, previous studies have established a complex interplay between the TRAIL pathway and immune function[31]. TRAIL has been shown to promote the activation of natural killer (NK) cells and cytotoxic T lymphocytes (CTLs) in tumors, contributing to tumor suppression[32,33]. Based on this evidence, we hypothesize that impaired immune function is a primary driver of poor prognosis in high-risk patients. To further explore this hypothesis, we analyzed the tumor immune microenvironment of osteosarcoma patients. Prognosis is significantly affected by dynamic changes in the tumor stroma and immune cell populations, which are key components of the tumor microenvironment[34]. We performed immune infiltration analysis using ESTIMATE and ssGSEA, revealing that patients with poor prognosis exhibited significantly lower StromalScore, ImmuneScore, and ESTIMATEScore, while TumorPurity was notably higher in comparison to patients with better outcomes. The ssGSEA analysis specifically examined immune cell composition and activity, identifying 25 immune cell types that significantly influenced osteosarcoma initiation and progression. These findings collectively underscore the crucial role of immune dysregulation in osteosarcoma prognosis and suggest that targeting immune pathways, particularly the TRAIL pathway, may provide therapeutic benefits for high-risk patients.

To further search for potential therapeutic targets, we conducted drug sensitivity analysis. The IC50 of a drug refers to its half maximal inhibitory concentration, which is a measure of its activity[35].In vitro drug screening, IC50 refers to the drug concentration required to inhibit 50% of cell growth or metabolic activity in a cell or tissue culture[36]. A lower IC50 value corresponds to higher drug sensitivity. We prioritized drugs with an average IC50 below 1 and, unexpectedly, identified paclitaxel as a promising candidate. Notably, patients in the high-risk (HR) group exhibited significantly lower IC50 values for paclitaxel, indicating enhanced sensitivity to this drug. Paclitaxel primarily exerts its anticancer effects by disrupting mitosis and inhibiting tumor cell proliferation[37], Given that the centrosome plays a crucial role in mitosis[38].Therefore, we believe that paclitaxel may exert its effects through centrosome-related genes. Hence, we conducted a molecular docking analysis to explore the potential interaction between paclitaxel and the protein produced by JTB gene. Through hydrogen bonding, we discovered that the interaction between JTB and paclitaxel has a binding affinity of − 5.5 kcal/mol. The presence and role of JTB in cancer are linked to the emergence, progression, and spread of different malignant tumors[39].

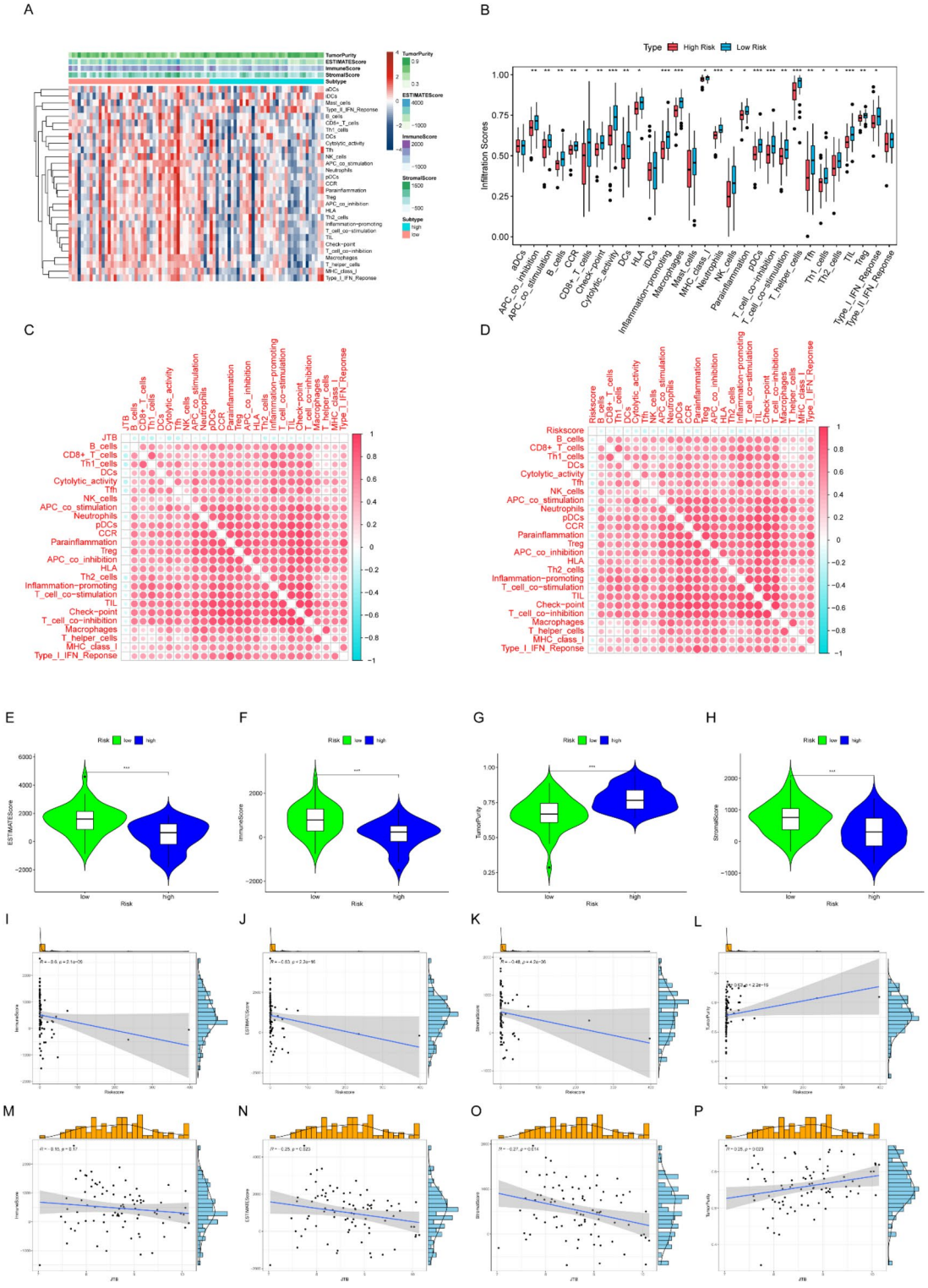


Several research studies indicate that the amount of JTB expression is notably increased in specific types of cancer, including breast cancer, liver cancer, and colon cancer[40,41]. Moreover, JTB is involved in biological processes such as cell proliferation, invasion, and tumor metastasis, making it an attractive therapeutic target. Recent studies suggest that JTB also influences immune cell function, contributing to tumor immune evasion, positioning it as a focal point in cancer immunotherapy research[42]. However, its impact on osteosarcoma remains unexplored. Based on our findings, we propose that paclitaxel exerts its effects by interacting with the JTB-encoded protein, thereby modulating JTB's biological activity. Given JTB's dual role in tumor cell division and immune regulation, its interaction with paclitaxel may have profound implications for osteosarcoma progression and patient prognosis. These findings provide novel insights into potential therapeutic strategies, suggesting that targeting JTB with paclitaxel could simultaneously impair tumor proliferation and restore immune function, thereby improving clinical outcomes for high-risk osteosarcoma patients.

◀**Fig. 7**. Immune infiltration analysis and correlation between immune-related factors and risk score. (**A**) Heatmap showing the distribution of immune cell infiltration levels between the high-risk and low-risk groups. The color gradient represents the relative abundance of immune cell populations. (**B**) Boxplot comparing immune infiltration scores for various immune cell types between the high-risk and low-risk groups. Significant differences are indicated (**$p<0.05$, **$p<0.01$, ***$p<0.001$). (**C**,**D**) Correlation heatmaps illustrate the relationships between immune-related factors and (**C**) JTB expression and (**D**) risk score, respectively. The color scale represents the strength of correlation coefficients. (**E**–**H**) Violin plots showing differences in immune score (**E**), stromal score (**F**), ESTIMATE score (b), and tumor purity (**H**) between high-risk and low-risk groups. Higher immune and stromal scores indicate a more immune-infiltrated tumor microenvironment. (**I**–**L**) Scatter plots depicting the correlation between the risk score and key immune-related features, including immune score (**I**), stromal score (**J**), ESTIMATE score (**K**), and tumor purity (**L**). Pearson correlation coefficients (R) and p-values are provided. (**M**–**P**) Scatter plots illustrating the correlation between JTB expression and key immune-related features, including immune score (**M**), stromal score (**N**), ESTIMATE score (**O**), and tumor purity (**P**).

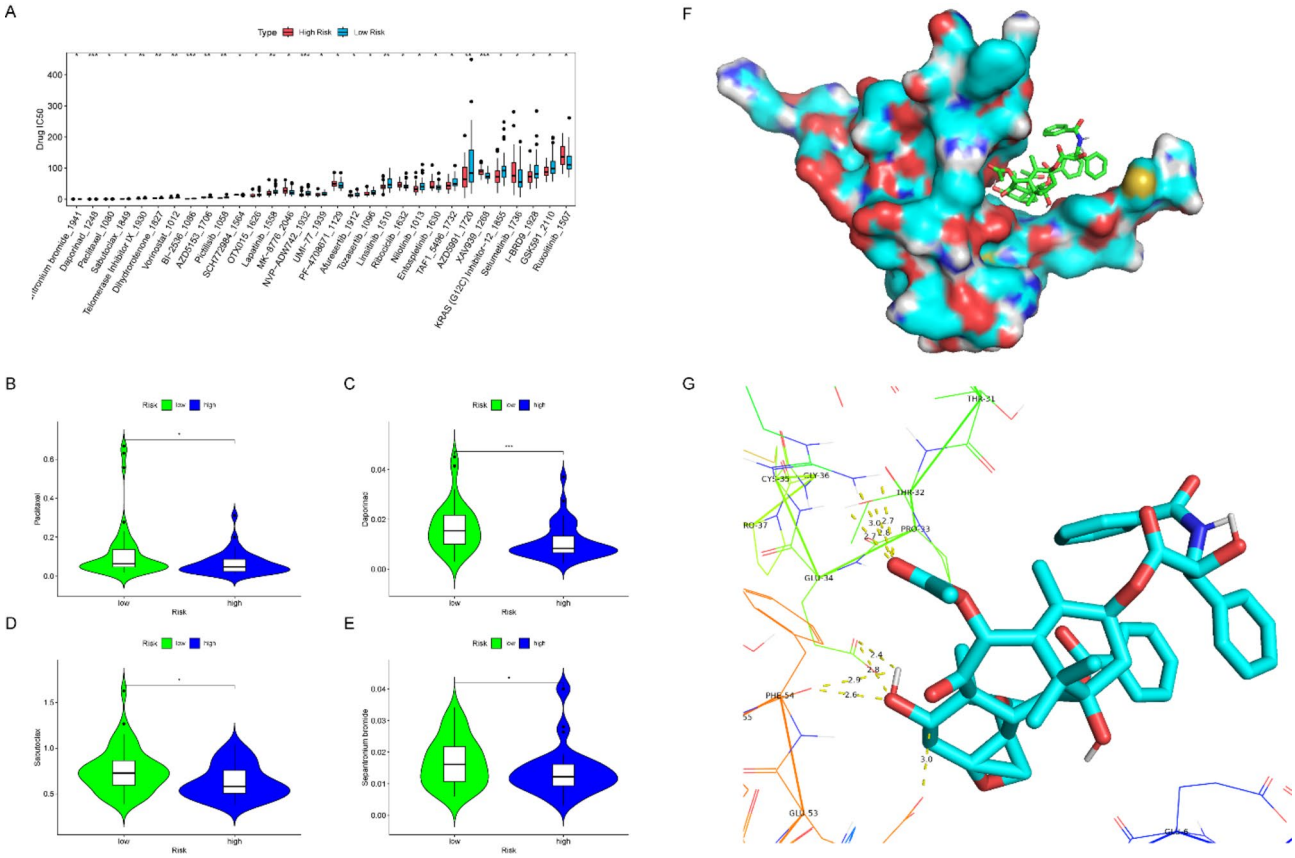


**Fig. 8**. The results of drug sensitivity and molecular docking analysis. (**A**) There were significant differences observed in the IC50 values of 31 drugs between the two groups. (**B**–**E**) There were four drugs with IC50 values less than 1. (**F**) The molecular docking analysis revealed the approximate binding site of paclitaxel with the JTB-encoded protein. (**G**) The results display the specific binding mode of paclitaxel with the JTB-encoded protein, including the amino acid residues involved in the binding.

To validate the findings from our bioinformatics analysis, we conducted laboratory experiments to examine the impact of JTB gene suppression in 143B osteosarcoma cells. Following si-JTB transfection, we observed a significant reduction in cell proliferation, with a portion of the cells undergoing apoptosis. Additionally, JTB knockdown markedly decreased the migratory and invasive capacities of 143B cells, further highlighting its role in tumor progression. Collectively, these results suggest that JTB plays a critical role in osteosarcoma cell proliferation and metastasis, reinforcing its potential as a therapeutic target for osteosarcoma treatment. We speculate that JTB may influence key tumor cell and immune cell functions, leading to alterations in cellular growth and metastatic behavior. The effectiveness of paclitaxel against osteosarcoma may be attributed to its ability to bind to JTB, resulting in JTB inactivation and subsequent activation of the TRAIL pathway, which enhances tumor cell apoptosis. Leveraging this mechanism may improve the therapeutic efficacy of paclitaxel in osteosarcoma treatment.

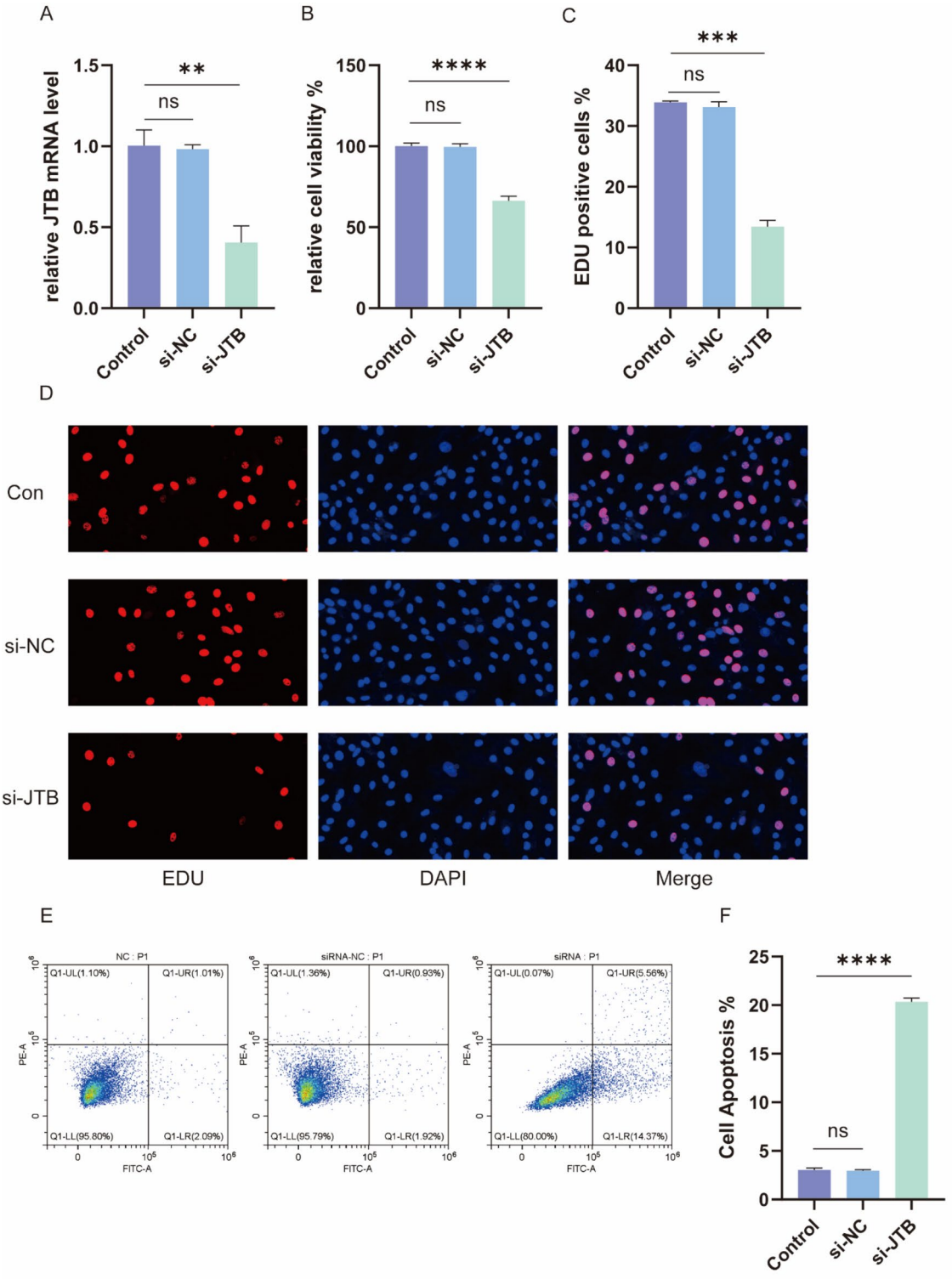


**Fig. 9**. JTB knockdown inhibited proliferation and promoted apoptosis in 143B cells. (**A**) qRT-PCR results show that si-JTB significantly reduced the transcription levels of JTB in 143B cells compared to control and si-NC groups. (**B**) Cell viability assay demonstrating that si-JTB treatment markedly decreased the relative viability of 143B cells. (**C**) Statistical analysis of EDU-positive cells revealed a significant reduction in proliferation capacity in 143B cells treated with si-JTB. (**D**) Representative immunofluorescence images of EDU staining showing a decrease in proliferating 143B cells in the si-JTB group compared to the control and si-NC groups. (**E**) Flow cytometry analysis illustrating an increase in apoptotic 143B cells following si-JTB treatment. (**F**) Quantitative analysis of apoptotic cells from flow cytometry results showing a significant elevation of apoptosis in the si-JTB group.

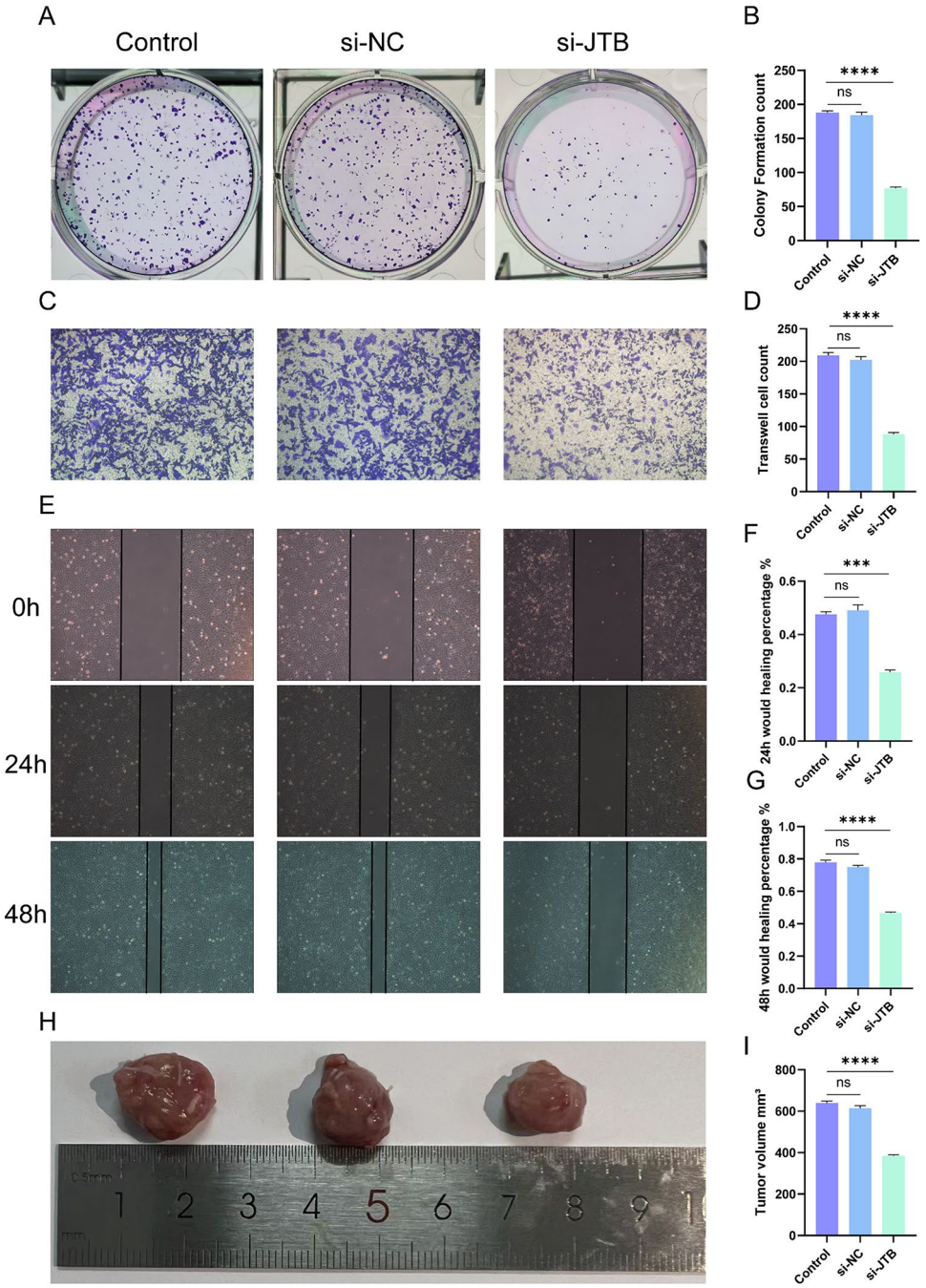


**Fig. 10**. Knockdown of JTB suppressed proliferation, migration, invasion, and tumor growth in 143B cells. (**A**) Colony formation assay images illustrating a reduction in colony numbers in the si-JTB group compared to the control and si-NC groups. (**B**) Quantitative analysis of colony numbers showed a significant decrease in the si-JTB group. (**C**) Representative images of the Transwell invasion assay showing fewer invaded cells in the si-JTB group compared to the control and si-NC groups. (**D**) Quantitative analysis of invaded cells demonstrated a significant reduction in invasion ability in the si-JTB group. (**E**) Wound healing assay images at 0 h, 24 h, and 48 h showing reduced migration in the si-JTB group compared to the control and si-NC groups. (**F**) Statistical analysis of the wound healing percentage at 24 h demonstrating reduced migration in the si-JTB group. (**G**) Statistical analysis of the wound healing percentage at 48 h confirming a further reduction in migration ability in the si-JTB group. (**H**) Representative images of tumors harvested from mice, showing smaller tumor sizes in the si-JTB group compared to control and si-NC groups. (**I**) Quantitative analysis of tumor volumes demonstrating a significant reduction in the si-JTB group.

However, our study has certain limitations. Due to the limited availability of clinical samples, we were unable to comprehensively investigate JTB expression alterations in human osteosarcoma and adjacent tissues. Additionally, our study did not fully elucidate the molecular mechanisms underlying JTB's role in osteosarcoma progression and immune regulation. Moving forward, we aim to expand our research to gain a more comprehensive understanding of these mechanisms, ultimately facilitating the development of targeted therapeutic strategies for osteosarcoma.

## Conclusion

In this study, we developed a centrosome-related prognostic model for osteosarcoma patients, providing a novel approach for risk stratification. Immune infiltration analysis revealed that high-risk patients exhibit impaired immune function, suggesting a potential link between centrosome-associated genes and immune dysregulation. Drug sensitivity analysis identified paclitaxel as a highly effective therapeutic agent, with the potential to improve prognosis by targeting both tumor cell mitosis and immune cell function. Our findings provide a robust predictive model for osteosarcoma prognosis while uncovering a previously unrecognized pathway and therapeutic target for paclitaxel-based treatment. These insights offer valuable guidance for clinical management, paving the way for personalized therapeutic strategies in osteosarcoma.

## Data availability

The study provides access to the datasets through online repositories. Below, you can find the repository/repositories' names and corresponding accession number(s): https://xenabrowser.net/datapages/.

Received: 18 November 2024; Accepted: 21 April 2025
Published online: 15 May 2025

## References

1. Ta, H. T., Dass, C. R., Choong, P. F. & Dunstan, D. E. Osteosarcoma treatment: state of the Art. *Cancer Metastasis Rev.* **28** (1–2), 247–263 (2009).
2. Corre, I., Verrecchia, F., Crenn, V., Redini, F. & Trichet, V. The osteosarcoma microenvironment: A complex but targetable ecosystem. *Cells*. **9**(4). (2020).
3. Ritter, J. & Bielack, S. S. Osteosarcoma *Ann. Oncol.* **21**(Suppl 7), vii320–325 (2010).
4. Jafari, F. et al. Osteosarcoma: A comprehensive review of management and treatment strategies. *Ann. Diagn. Pathol.* **49**, 151654 (2020).
5. Meltzer, P. S. & Helman, L. J. New horizons in the treatment of osteosarcoma. *N. Engl. J. Med.* **385** (22), 2066–2076 (2021).
6. Lilienthal, I. & Herold, N. Targeting molecular mechanisms underlying treatment efficacy and resistance in osteosarcoma: A review of current and future strategies. *Int. J. Mol. Sci.* **21**(18). (2020).
7. Chen, C. et al. Immunotherapy for osteosarcoma: fundamental mechanism, rationale, and recent breakthroughs. *Cancer Lett.* **500**, 1–10 (2021).
8. Harrison, D. J., Geller, D. S., Gill, J. D., Lewis, V. O. & Gorlick, R. Current and future therapeutic approaches for osteosarcoma. *Expert Rev. Anticancer Ther.* **18** (1), 39–50 (2018).
9. Vasquez-Limeta, A. & Loncarek, J. Human centrosome organization and function in interphase and mitosis. *Semin. Cell. Dev. Biol.* **117**, 30–41 (2021).
10. Zhao, J. Z., Ye, Q., Wang, L. & Lee, S. C. Centrosome amplification in cancer and cancer-associated human diseases. *Biochim. Biophys. Acta Rev. Cancer*. **1876** (1), 188566 (2021).
11. Remo, A., Li, X., Schiebel, E. & Pancione, M. The centrosome linker and its role in cancer and genetic disorders. *Trends Mol. Med.* **26** (4), 380–393 (2020).
12. Yeow, Z. Y. et al. Targeting TRIM37-driven centrosome dysfunction in 17q23-amplified breast cancer. *Nature* **585** (7825), 447–452 (2020).
13. Wang, W., Zhang, J., Wang, Y., Xu, Y. & Zhang, S. Identifies microtubule-binding protein CSPP1 as a novel cancer biomarker associated with ferroptosis and tumor microenvironment. *Comput. Struct. Biotechnol. J.* **20**, 3322–3335 (2022).
14. Gajewski, T. F., Schreiber, H. & Fu, Y. X. Innate and adaptive immune cells in the tumor microenvironment. *Nat. Immunol.* **14** (10), 1014–1022 (2013).
15. Oved, J. H., Barrett, D. M. & Teachey, D. T. Cellular therapy: Immune-related complications. *Immunol. Rev.* **290** (1), 114–126 (2019).
16. Pan, K. et al. CAR race to cancer immunotherapy: from CAR T, CAR NK to CAR macrophage therapy. *J. Exp. Clin. Cancer Res.* **41** (1), 119 (2022).
17. Marzagalli, M., Ebelt, N. D. & Manuel, E. R. Unraveling the crosstalk between melanoma and immune cells in the tumor microenvironment. *Semin. Cancer Biol.* **59**, 236–250 (2019).
18. Chen, L. et al. CAR-T cell therapy for lung cancer: potential and perspective. *Thorac. Cancer*. **13** (7), 889–899 (2022).
19. Yang, Y. H., Liu, J. W., Lu, C. & Wei, J. F. CAR-T cell therapy for breast cancer: from basic research to clinical application. *Int. J. Biol. Sci.* **18** (6), 2609–2626 (2022).
20. Lei, X. et al. Immune cells within the tumor microenvironment: biological functions and roles in cancer immunotherapy. *Cancer Lett.* **470**, 126–133 (2020).
21. Fang, Z., Gao, Z. J., Yu, X., Sun, S. R. & Yao, F. Identification of a centrosome-related prognostic signature for breast cancer. *Front. Oncol.* **13**, 1138049 (2023).
22. Kanehisa, M., Furumichi, M., Sato, Y., Matsuura, Y. & Ishiguro-Watanabe, M. KEGG: biological systems database as a model of the real world. *Nucleic Acids Res.* **53** (D1), D672–D677 (2025).
23. Kanehisa, M. Toward Understanding the origin and evolution of cellular organisms. *Protein Sci.* **28** (11), 1947–1951 (2019).
24. Kanehisa, M. & Goto, S. KEGG: Kyoto encyclopedia of genes and genomes. *Nucleic Acids Res.* **28** (1), 27–30 (2000).
25. Lee, J. A. et al. Osteosarcoma in adolescents and young adults. *Cells*. **10**(10). (2021).
26. Zhang, X. & Guan, Z. PET/CT in the diagnosis and prognosis of osteosarcoma. *Front. Biosci. (Landmark Ed)*. **23** (11), 2157–2165 (2018).
27. Priyanga, J., Guha, G. & Bhakta-Guha, D. Microtubule motors in centrosome homeostasis: A target for cancer therapy? *Biochim. Biophys. Acta Rev. Cancer*. **1875** (2), 188524 (2021).
28. Sun, B. et al. Traditional Chinese medicines and their active ingredients sensitize cancer cells to TRAIL-induced apoptosis. *J. Zhejiang Univ. Sci. B.* **22** (3), 190–203 (2021).

29. von Karstedt, S., Montinaro, A. & Walczak, H. Exploring the trails less travelled: TRAIL in cancer biology and therapy. *Nat. Rev. Cancer*. **17** (6), 352–366 (2017).
30. Wong, S. H. M. et al. The TRAIL to cancer therapy: hindrances and potential solutions. *Crit. Rev. Oncol. Hematol.* **143**, 81–94 (2019).
31. Cardoso Alves, L., Corazza, N., Micheau, O. & Krebs, P. The multifaceted role of TRAIL signaling in cancer and immunity. *FEBS J.* **288** (19), 5530–5554 (2021).
32. Cardoso Alves, L. et al. Non-apoptotic TRAIL function modulates NK cell activity during viral infection. *EMBO Rep.* **21** (1), e48789 (2020).
33. Nai, Y. et al. TRAIL-R1-targeted CAR-T cells exhibit dual antitumor efficacy. *Front. Mol. Biosci.* **8**, 756599 (2021).
34. Hinshaw, D. C. & Shevde, L. A. The tumor microenvironment innately modulates cancer progression. *Cancer Res.* **79** (18), 4557–4566 (2019).
35. Park, A. et al. A comprehensive evaluation of regression-based drug responsiveness prediction models, using cell viability inhibitory concentrations (IC50 values). *Bioinformatics*. **38** (10), 2810–2817 (2022).
36. Yucha, R. W. et al. In vitro drug-induced liver injury prediction: criteria optimization of efflux transporter IC50 and physicochemical properties. *Toxicol. Sci.* **157** (2), 487–499 (2017).
37. Zhu, L. & Chen, L. Progress in research on paclitaxel and tumor immunotherapy. *Cell. Mol. Biol. Lett.* **24**, 40 (2019).
38. Sakai, H. & Ohta, K. Centrosome signalling at mitosis. *Cell. Signal.* **3** (4), 267–272 (1991).
39. Kanome, T. et al. Characterization of jumping translocation breakpoint (JTB) gene product isolated as a TGF-beta1-inducible clone involved in regulation of mitochondrial function, cell growth and cell death. *Oncogene* **26** (41), 5991–6001 (2007).
40. Jayathirtha, M. et al. Investigating the function of human jumping translocation breakpoint protein (hJTB) and its interacting partners through In-Solution proteomics of MCF7 cells. *Molecules*. **27**(23). (2022).
41. Pan, J. S. et al. Interacting with HBsAg compromises resistance of jumping translocation breakpoint protein to ultraviolet radiation-induced apoptosis in 293FT cells. *Cancer Lett.* **285** (2), 151–156 (2009).
42. Hwang, I. Y., Park, C. & Kehrl, J. H. Impaired trafficking of Gnai2+/- and Gnai2-/- T lymphocytes: implications for T cell movement within lymph nodes. *J. Immunol.* **179** (1), 439–448 (2007).


## Author contributions

Yj.Z. and K.T. designed and conducted the experiments, analyzed the data, and wrote the manuscript. Bh.G. was responsible for sample collection, data processing, and statistical analysis. L.L. provided technical support and assisted in experimental design. Qj.W. supervised the study, provided critical revisions to the manuscript, and guided data interpretation. Y.H. conceptualized the study, secured funding, and oversaw the overall research direction and execution. All authors reviewed and approved the final manuscript.

## Funding

The current research is funded by the Hubei province science Foundation for Young Scientists (Grant No.2023AFB255).

## Declarations

## Competing interests

The authors declare no competing interests.

## Ethics statement

This study was conducted in accordance with the ARRIVE guidelines (https://arriveguidelines.org). All animal procedures were approved by the Animal Ethics Committee of Renmin Hospital of Wuhan University (No. 202300255) and performed in compliance with institutional and national ethical standards.

## Additional information

**Supplementary Information** The online version contains supplementary material available at https://doi.org/10.1038/s41598-025-99419-5.

**Correspondence** and requests for materials should be addressed to Q.W. or Y.H.